Pure & Appl. Chem., Vol. 64, No. 5, pp. 685–689, 1992.
Printed in Great Britain.

Diagnostics of plasmas by CARS (coherent anti-Stokes Raman scattering)

M. Lefebvre, M. Péalat and J.P. Taran

Office National d'Etudes et de Recherches Aérospatiales
29, avenue de la Division Leclerc, 92320 Châtillon, France

Abstract – Some of the most representative results of the coherent anti-Stokes Raman spectroscopy research program on discharges at ONERA are presented. A very short review of the principles of CARS and of the main instrumental characteristics is first given. The results of an analysis of a magnetic multipole-confined H_2 discharge are then shown. The kinetics of rotational and vibrational state populations have been followed in the transient regime and the deactivation of the vibrational level v = 1 by the walls measured. Also, O_2 in a glow discharge and in a waveguide discharge has been studied. Rotational, vibrational temperatures and the density of the $^1\Delta$ state have been monitored as functions of position, pressure and discharge current.

INTRODUCTION

Low temperature plasmas and discharges are generally highly displaced from equilibrium. Their characterization requires quantum-state specific, non-intrusive optical measurements. For a long time, only absorption and emission spectroscopies were available, and much about discharged gases has been learned thanks to these methods. The past 10-15 years have seen the introduction of more attractive laser-based light-scattering techniques such as Laser-Induced Fluorescence (LIF) or Coherent Anti-Stokes Raman Scattering (CARS). These offer the additional advantage of spatial resolution and, for CARS, extreme luminosity and background rejection (ref. 1). While conventional CARS performed with a fixed frequency, frequency doubled Nd:YAG laser, does not quite possess the sensitivity of LIF, its limited requirements with regard to optical access make it the most flexible general purpose tool for plasma diagnostics.

The first application of CARS in a discharge was demonstrated as early as 1977 (ref. 2). Since, many systematic studies of homonuclear diatomics in various types of discharge configurations have been performed. Some of the salient results obtained at ONERA are reported here.

EXPERIMENTAL SET-UP

It is not the purpose of this communication to present a detailed review of the principles of CARS and a description of the ONERA instrument, both of which can be found in previous publications (ref. 1, 3). To summarize, CARS can be observed when two collinear light beams with frequencies ω_1 and ω_2 (hereafter called laser and Stokes respectively, with $\omega_1 > \omega_2$), traverse a sample with a Raman active vibrational mode of frequency $\omega_v = \omega_1 - \omega_2$. A new wave is then generated at the anti-Stokes frequency $\omega_3 = \omega_1 + (\omega_1 - \omega_2) = 2\,\omega_1 - \omega_2$ in the forward direction, and collinear with the pump beams (Fig. 1).

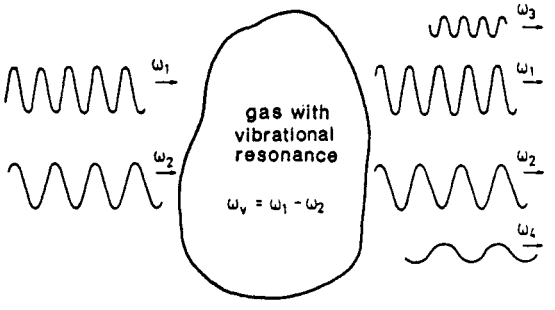

Figure 1 - CARS and CSRS

This new wave results from the inelastic scattering of the wave at ω_1 by the molecular vibrations, which are coherently driven by the waves at ω_1 and ω_2 (hence the name of the effect). We note that the same mechanism creates a similar wave at $2\,\omega_2 - \omega_1$ (CSRS for Coherent Stokes Raman Scattering). This wave has been observed and is sometimes used for spectroscopic purposes, in spite of the difficulties connected with background light rejection and poorer detector efficiencies.

Scanning the frequency ω_2 and monitoring the signal amplitude at ω_3, with ω_1 kept fixed, allows one to recognize the various molecular vibrational resonances and hence to identify the chemical components and to perform quantum state-selected number density measurements. This is the basis of the application of CARS to analytical chemistry and temperature measurements. Also, note that the beams are generally focused to a point, where signal generation is much more intense. This provides some spatial resolution.

The instrument is based on the use of a single-mode pulsed Nd:YAG laser which is frequency-doubled to 532 nm. This laser delivers the ω_1 frequency and is also used to pump the tunable dye laser which emits the ω_2 frequency. These lasers have a pulse duration of about 10 ns, and energies of 50 mJ and 3 mJ respectively. The detection of the anti-Stokes signals is done via dichroic filters and specialized monochromators (to block off the pumps beams), and photomultiplier tubes. Scanning the spectrum of the molecule of interest necessitates several minutes.

The detection sensitivity is in the range of $10^{11} - 10^{13}$ cm^{-3} per quantum state depending on the species and the static temperature.

RESULTS

H_2 in magnetic multipolar discharge

The analysis of a low-pressure discharge with magnetic multipolar confinement of primary electrons emitted by a tungsten filament has begun several years ago in our laboratory (ref. 3). Note that these sources are interesting for the production of H^- ions (ref. 4). Measurements were done in a 16 cm-dia., 20 cm-high reactor, at 55 µbar pressure, and using a 90 V, 10 A discharge. The main conclusions of these previous studies are the following :

1) the rotational distribution strongly deviates from the Boltzmann law for $J \geq 5$; the rotational temperature deduced from $J < 5$ is about 530 K ;

2) the vibrational distribution nearly obeys the Boltzmann law up to $v = 3$, highest vibrational level detected ; the vibrational temperature is about 2400 K ;

3) the H_2 partial pressure is about 70 % of the pressure measured by the gauge, indicating some level of dissociation ;

4) the atomic fraction of H atoms is small ($\approx$ 5 %), but their apparent translational temperature is high ($\approx$ 3500 K), yielding a high partial pressure.

New measurements have been attempted to assess the inhomogeneities within the reactor and the kinetics of molecular excitation by electrons and relaxation by walls (ref. 4). These are illustrated in Figures 2-4. Excitation was either by a steady-state discharge of 10 A, 90 V or by rectangular discharge pulses, also of 10 A, 90 V, with 1 ms duration.

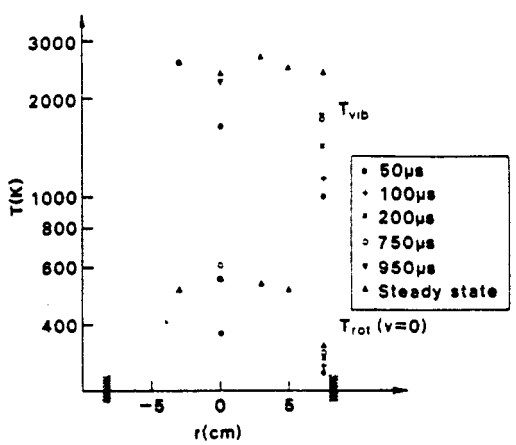

Figure 2 - Radial profiles and temporal response of rotational and vibrational temperatures. The origin of times is the front edge of discharge pulse ; pressure : 5.3 Pa

Figure 2 presents the radial steady-state distributions of the vibrational and rotational temperatures and their rise under excitation by the pulse leading edge. The difference between them is striking, as the rotational temperature presents a strong gradient between the center and the wall, while the vibrational distribution is flat. This is caused by the difference in deactivation rates at the wall. The rotational temperature is determined from the ratio of populations in rotational states J = 1 and J = 3 of vibrational level v = 0 and the vibrational temperature is derived from the radio of populations in states (J = 1, v = 1) and (J = 1, v = 0).

The difference in behaviour of the rotation and vibration is striking at steady state, since a strong gradient from the center to the walls is observed for the rotational temperature while the vibrational temperature is uniform. This is because the vibration is a little relaxed by the wall collisions in comparison with the rates of excitation by electrons and relaxation by atoms in the volume of the reactor ; on the contrary, the accommodation of the rotation (and translation) at the walls is very strong compared with the rate of heating by electronic collisions. With regard to the rotation, an interesting phenomenon was also revealed by the state-resolved measurements (Fig. 3). The early part of the pulsed discharge causes a rapid deviation from the Boltzmann law for the ortho and para H_2 up to J = 3. This is probably because cross-sections for rotational heating of H_2 by electrons are higher for the para than the ortho (ref. 6).

Finally, the behaviour of the vibration under excitation by a 1 ms square discharge pulse was studied at a pressure of 0.5 Pa (Fig. 4). Of particular interest is the decay of the vibrational temperature at switch-off. Since relaxation is primarily caused by wall collisions, it has been possible to evaluate the probability of deactivation : about 16 collisions at the wall are necessary to deexcite v = 1. This parameter is important for the design of these sources of H^- ions.

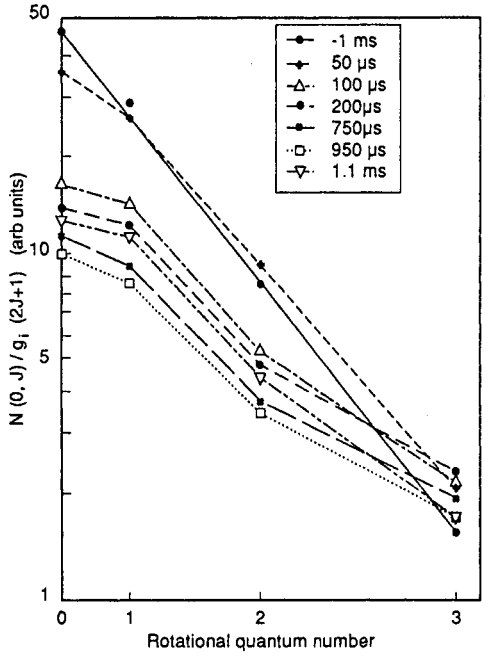

Figure 3 - Boltzmann plots of rotational state densities in v = 0 for 2.76 Pa and at different times after switch-on

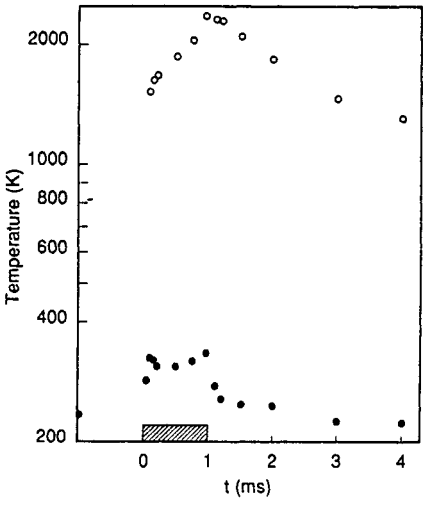

Figure 4 - Rise and decay of rotational temperature T_{rot} (v = 0) (•) and vibrational temperature T_{vib} (o) at the center of the generator and for 0.53 Pa with 1-ms-long discharge pulse (shown by hatched rectangle).

O_2 in glow and surfatron discharges

The behaviour of the $^3\Sigma$ state of O_2 in discharges has been monitored in a similar manner. The $^1\Delta$ metastable state has also been detected and its rotational temperature measured.

The main results are presented in Fig. 5 to 7 for the glow discharge (ref. 7). The latter was made in a 16-mm id, air-cooled tube. The radial profiles of rotational temperature T_R and vibrational temperature T_v are plotted in Fig. 5. They show that T_R and T_v, which are almost equal except at the lower pressure, increase with discharge current I and pressure P ; the rotation is also well "accommodated" at the wall, while the vibration is always

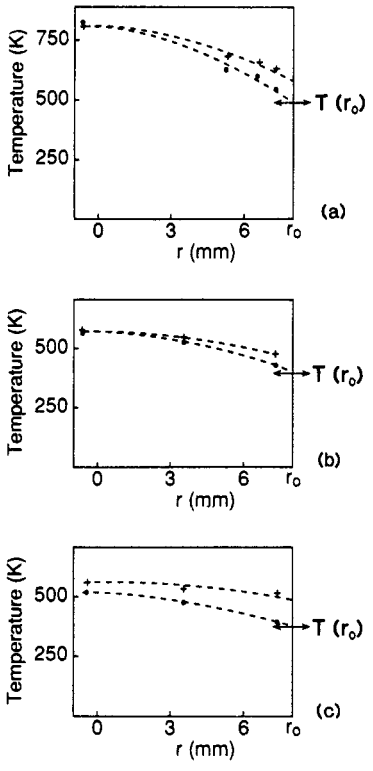

Figure 5 - Radial profiles of temperatures of rotation (•) and vibration (+) ; r_0 : wall position ; T (r_0) : wall temperature ; (a) : 625 Pa, 80 mA ; (b) : 625 Pa, 30 mA ; (c) : 125 Pa, 80 mA

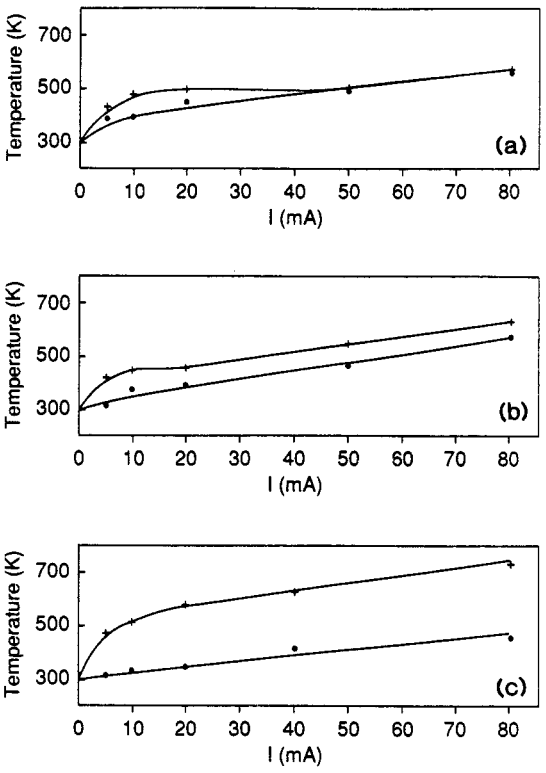

Figure 6 - Rotational (•) and vibrational (+) temperatures vs discharge current I ; (a) : 312.5 Pa ; (b) : 125 Pa ; (c) : 62.5 Pa ; position : r = 0

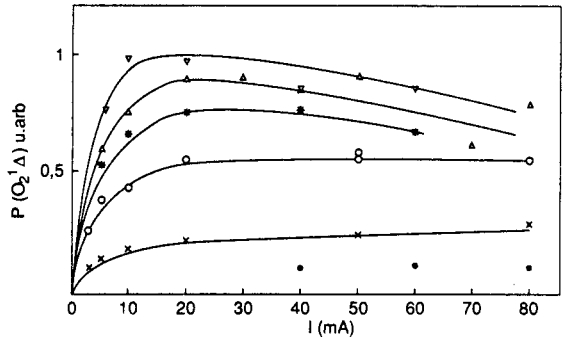

Figure 7 - Partial pressure in arbitrary units of $^1\Delta$ state vs current I and pressure P : 62.5 Pa (•) ; 125 Pa (×) ; 312.5 Pa (O) ; 500 Pa (*) ; 625 Pa (Δ) ; 750 Pa (∇)

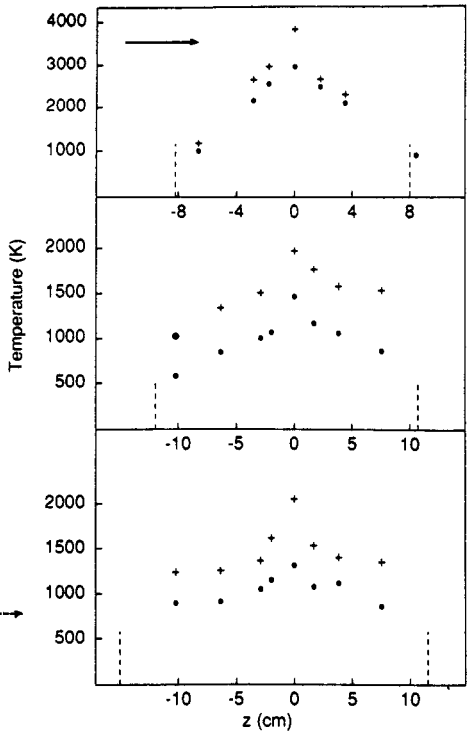

Figure 8 - Axial profiles of T_R (•) and T_v (+). Dashed lines mark the ends of the discharge and the arrow the flow direction. Pressure, discharge power, and volumetric flow rate $\dot{v}$ are, respectively : (a) : 625 Pa, 1000 W, 200 cm^3/min ; (b) : 125 Pa, 340 W, 190 cm^3/min ; (c) : 125 Pa, 340 W, 10 cm^3/min

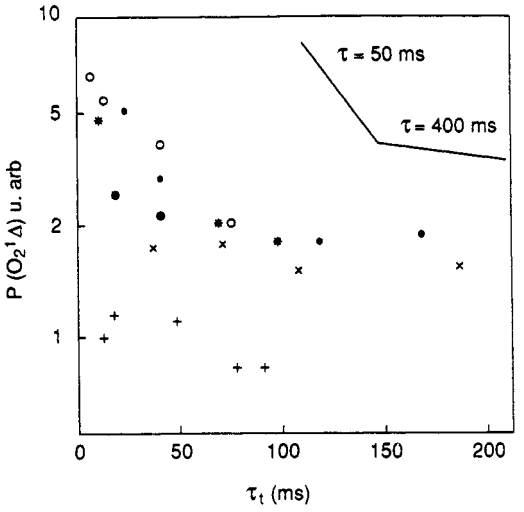

Figure 9 - Partial pressure of O_2 $^1\Delta$ in post-discharge vs time elapsed since leaving the discharge and volumetric flow rate $\dot{v}$. Characteristic slopes for two decay times are shown in top right corner ;
P = 62.5 Pa, $\dot{v}$ = 50 cm³/mn (+) ;
P = 120 Pa, $\dot{v}$ = 100 cm³/mn (*) ;
P = 120 Pa, $\dot{v}$ = 50 cm³/mn (×) ;
P = 240 Pa, $\dot{v}$ = 100 cm³/mn (•) ;
P = 240 Pa, $\dot{v}$ = 300 cm³/mn (O).

slightly hotter. It has been verified that vibrational states v = 0 – 2 obey the Boltzmann law. Fig. 6 (a-c) explores the behaviour of T_V and T_R on the tube axis, when the pressure is lowered and the current increases. While the two temperatures are seen to equilibrate at high P and I, they separate significantly (250 K) at the lowest pressure. These behaviours are attributed to the growth of the 0 atom density when I and P increase. Fig. 7 presents the evolution of the partial pressure of the $^1\Delta$ O_2 state vs the same parameters, also measured at r = 0. Because no calibration was possible for this metastable state, the results are presented in arbitrary units.

Radial and axial profiles of the temperatures and the axial distribution of O_2 $^1\Delta$ were measured. Figure 8 gives the axial values of T_R and T_V for various flow rates and discharge powers. A pronounced increase of the two parameters is noticed at the center of the gap. A slight asymmetry is also visible. Atoms are likely to play an important role in the deactivation of the vibration ; since their formation is slow, fast flows experience less O formation, hence higher T_V. Finally, the O_2 $^1\Delta$ density axial profiles have been replotted as a function of time elapsed since leaving the discharge, using the known flow velocity (Fig. 9). Note that the detection sensitivity was insufficient for detection of that species in the discharge. One observes that at pressures below 120 Pa, the decay of $^1\Delta$ density is slow (0.4 s). At higher pressure, two decay times are apparent : the decay is first rapid (50 ms), followed by the slower decay which is seen at the low pressures. These behaviours indicate two deexcitation mechanisms : first, rapid volume quenching by species formed in the discharge (presumably, O), then, slower deactivation by walls. Modelling for these phenomena remains to be done.

CONCLUSION

CARS is unquestionably a powerful technique for species detection and temperature measurement in discharges. It does not quite have the sensitivity of LIF, but its variant, resonance-enhanced CARS (ref. 1) will soon provide gain in sensitivity 10^2-10^3 times superior ; this will compare favorably with LIF and will offer, in addition, the same stray light discrimination ability which is typical of coherent non-linear spectroscopic methods.

REFERENCES

[1] S.A.J. Druet and J.P. Taran, Prog. Quant. Elec. 7, 1-72 (1981).

[2] W.M. Tolles, J.W. Nibler, J.R. Mc Donald and A.B. Harvey, Appl. Spectroscopy 31, 253 (1977).

[3] M. Péalat, J.P. Taran, M. Bacal and F. Hillion, J. Chem. Phys. 82, 4943 (1985).

[4] W.B. Kunkel, IEEE Trans. Nucl. Sci. 26, 4166 (1979).

[5] M. Lefebvre, M. Péalat, J.P. Taran, P. Berlemont, M. Bacal, D.A. Skinner, J. Bretagne and R.J. Hutcheon, "Coherent Anti-Stokes Raman Scattering Study of the Dynamics of a Multipolar Plasma Generator", (to be published).

[6] N.F. Lane, Rev. Mod. Phys. 52, 29 (1980).

[7] M. Touzeau, M. Vialle, Zellagui, G. Gousset, M. Lefebvre and M. Péalat, J. Phys. D : Appl. Phys. 24, 41 (1991).